JOURNAL OF COMPUTATIONAL PHYSICS 74, 143–176 (1988)

Assessment of Finite Difference Approximations for the Advection Terms in the Simulation of Practical Flow Problems

M. A. R. SHARIF AND AHMED A. BUSNAINA

Department of Mechanical and Industrial Engineering, Clarkson University, Potsdam, New York 13676

Received April 18, 1986; revised March 20, 1987

An assessment of seven discretization schemes for the advection terms of the transport equation to reduce numerical diffusion in practical flow problems has been established. The schemes have been evaluated using three test cases for laminar flow problems. The test cases consist of the transport of a scalar step in a uniform velocity field, two interacting parallel streams, and a slot jet. The performance of the schemes is evaluated for advection-dominated flows in transient and steady-state solutions. The considered schemes include four that have not been evaluated before for practical flow problems. In general, schemes which produced less numerical diffusion suffered from more numerical dispersion or oscillations. Two bounding techniques considered in the study were effective in significantly elliminating numerical dispersion.

1. INTRODUCTION

1.1. *The Problem*

Artificial damping or numerical diffusion presents a very serious problem to computational fluid dynamicists. Computational fluid dynamics codes are widely used in the aerospace industry for the design of gas turbine engine components including combustors, compressors, and turbines. Most available codes, however, suffer from the numerical diffusion problem. Numerical diffusion makes modelling of practical and complex flow problems very difficult by masking the physics of the problem. The main source of the artificial diffusion arises from discretizing the advection terms in the transport equations. Central differencing, which is second-order accurate, is useless for flow situations with Peclet number higher than 2 where oscillatory behavior or nonconvergence occurs. Therefore, for the sake of obtaining a stable solution the upwind differencing is usually utilized with the unfortunate introduction of numerical diffusion and the severe inaccuracies it presents. These errors are typically associated with the one-sided upstream differencing of the advective terms. Several other schemes for discretizing the advection terms have been proposed and evaluated. A more recent assessment of finite difference methods was presented by Syed *et al.* [1, 2] where five schemes were evaluated. The schemes

0021-9991/88 $3.00

581/74/1-10

were: skew, quadratic, Agarwal, spline, and Hermitian differencing schemes. He concluded that the skew upwind scheme was the most accurate of the five. Some problems were encountered, however, with that scheme where overshoot and unbounded solutions were experienced and the scheme had to be bounded. The above mentioned study [1, 2] did not examine the differencing schemes for time-dependent flow computations. Two similar studies by Leschziner [3] and Shyy [4] evaluated various finite-difference techniques for steady-state advection-dominated flow problems. Leschziner [3] examined the hybird central/upwind, hybird central/skew-upwind, and quadratic upstream-weighted differencing schemes. The study concluded that the last two schemes yield similar results which are superior to those obtained with the first scheme. Leschziner also reported that the two superior schemes suffered from a limited unboundedness problem. Shyy [4] studied five different schemes; first-order upwind, skew upwind, second-order upwind, central differencing, and quadratic upwind. The study indicated that the second-order upwind is the most satisfactory. The second-order upwind scheme had been found, however, to exhibit limited overshoot in the solution [4].

1.2. *The Present Contribution*

The present paper evaluates seven finite differencing schemes for the advection terms. The evaluation process is based on three practical test cases. The selected schemes are:

1. Weighted upwind differencing (WUD) [5].
2. A predictor-corrector style second order upwind differencing (SOUD1) [6].
3. Second-order upwind differencing (SOUD2) [4].
4. Skew upwind differencing (SUD) [7].
5. Transportive upwind differencing (TUD) [8].
6. Directional transportive upwind differencing (DTUD) [8].
7. Quadratic upwind interpolation differencing (QUID) [9].

Four of the investigated schemes (2, 3, 5, and 6) have not been tested before for practical flow problems.

2. Computational Analysis

2.1. *The Technique*

The computational procedure solves directly for the primitive pressure and velocity variables and is based on the Marker and Cell (MAC, Los Alamos) technique. This is one of the most well-known methods to solve time-dependent incompressible fluid flow problems. This work is based upon a two-dimensional version [5, 10] of it. In the present work, an Eulerian finite difference formulation is used

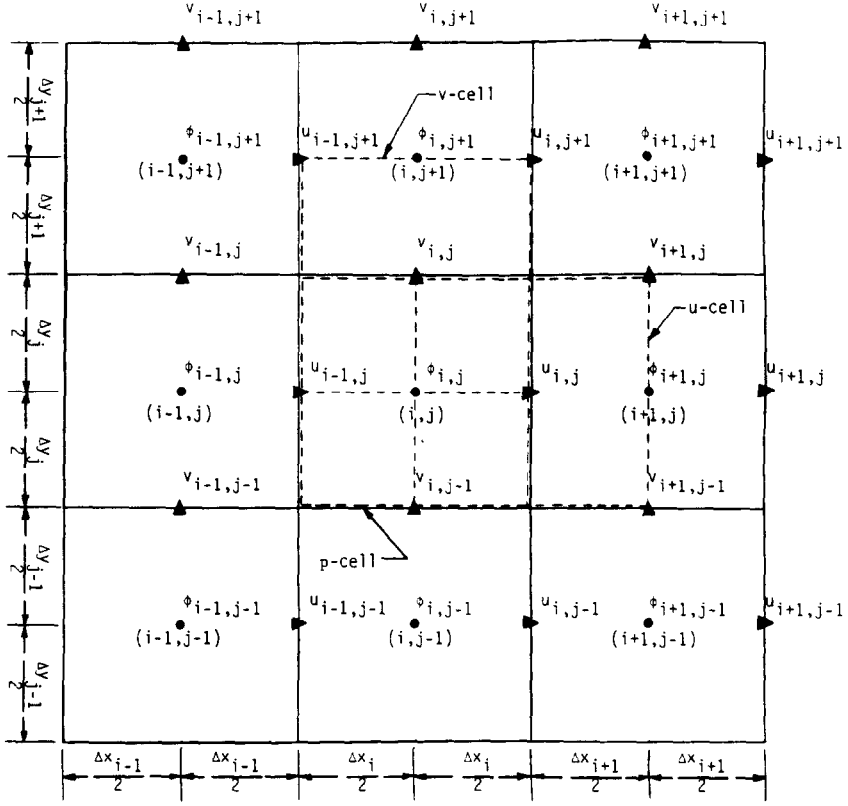

FIG. 1. Schematic of the grid system showing the control volumes for different variables.

with pressure and velocity as the main dependent variables. Figure 1 illustrates the total staggered mesh arrangement exhibiting the computational cells and shows the location of each of the field variables p, u, and v and its corresponding (i, j)-cells. Normal velocities in this particular grid system lie directly on the physical boundaries of the solution domain, while the tangential velocities and pressure are displaced half a cell interval inside the flowfield. In this way the exterior fictitious cells are particularly convenient when applying the boundary conditions.

2.2. *The Governing Equations*

The governing equations of the incompressible flow field are the continuity equation, the conservation of momentum in the x and y directions, and the scalar transport equation. These may be taken in Cartesian coordinates in the conservative form [5, 10] as

$$\text{continuity:} \qquad \frac{\partial u}{\partial x}+\frac{\partial v}{\partial y}=0 \tag{1}$$

$$x\text{-momentum:} \quad \frac{\partial u}{\partial t}+\frac{\partial(uu)}{\partial x}+\frac{\partial(vu)}{\partial y}=-\frac{\partial p}{\partial x}+\nu\left(\frac{\partial^2 u}{\partial x^2}+\frac{\partial^2 u}{\partial y^2}\right) \tag{2}$$

$$y\text{-momentum:} \quad \frac{\partial v}{\partial t}+\frac{\partial(uv)}{\partial x}+\frac{\partial(vv)}{\partial y}=-\frac{\partial p}{\partial y}+\nu\left(\frac{\partial^2 v}{\partial x^2}+\frac{\partial^2 v}{\partial y^2}\right) \tag{3}$$

$$\text{scalar transport:} \quad \frac{\partial \phi}{\partial t}+\frac{\partial(u\phi)}{\partial x}+\frac{\partial(v\phi)}{\partial y}=\Gamma_\phi\left(\frac{\partial^2 \phi}{\partial x^2}+\frac{\partial^2 \phi}{\partial y^2}\right), \tag{4}$$

where u and v are x and y components of velocity, t is the time, p is the ratio of pressure to the constant density ρ, ν is the kinematic viscosity, and Γ_ϕ is the coefficient of diffusivity for the scalar ϕ.

2.3. *The Finite Difference Equations*

In formulating the finite difference representations of the governing partial differential equations, central differencing is used for the diffusion and pressure terms and forward differencing is used for time. All the expressions are given for a general nonuniform grid.

The advection terms in the transport equations for all the investigated schemes can be expressed in the general form presented below. The notations *UL*, *VL*, *UR*, *VR*, *UB*, *VB*, *UT*, and *VT* for the advecting velocity components at the cell faces apply for any of the *u*-, *v*-, or *p*-cell. *U* and *V* denote the x and y components of velocity where *L*, *R*, *B*, and *T* imply left, right, bottom, and top face of the cell, respectively. These may be interpolated from the appropriate velocity components surrounding the cell face or may be located on the cell face itself.

Considering the *u*-cell, the advection terms of the x-momentum equation are given in the conservative form as;

$$DUUDX=\left.\frac{\partial(uu)}{\partial x}\right|_{i,j}=\frac{(UR)(URW)-(UL)(ULW)}{(1/2)(\Delta x_i+\Delta x_{i+1})} \tag{5}$$

$$DVUDY=\left.\frac{\partial(vu)}{\partial y}\right|_{i,j}=\frac{(VT)(UTW)-(VB)(UBW)}{\Delta y_j}, \tag{6}$$

where *URW*, *ULW*, *UTW*, and *UBW* are the interpolated values of the x-component of velocity at some upstream location which depends on the particular scheme employed. The interpolation method for each scheme will be discussed in Section 3.

Considering the *v*-cell the advective terms for the y-momentum equation are given in the conservative form as

$$DUVDX=\left.\frac{\partial(uv)}{\partial x}\right|_{i,j}=\frac{(UR)(VRW)-(UL)(VLW)}{\Delta x_i} \tag{7}$$

$$DVVDY=\left.\frac{\partial(vv)}{\partial y}\right|_{i,j}=\frac{(VT)(VTW)-(VB)(VBW)}{(1/2)(\Delta y_j+\Delta y_{j+1})}, \tag{8}$$

where *VRW*, *VLW*, *VTW*, and *VBW* are the interpolated values of the y-component of velocity at some upstream location which depends on the particular scheme employed.

Considering the p-cell, the advective terms for the scalar transport equation are given in the conservative form as

$$DUFDX = \left.\frac{\partial(u\phi)}{\partial x}\right|_{i,j} = \frac{(UR)(\phi RW) - (UL)(\phi LW)}{\Delta x_i} \tag{9}$$

$$DVFDY = \left.\frac{\partial(v\phi)}{\partial y}\right|_{i,j} = \frac{(VT)(\phi TW) - (VB)(\phi BW)}{\Delta y_j}, \tag{10}$$

where ϕRW, ϕLW, ϕTW, and ϕBW are interpolated values of the scalar at some upstream location which depends on the particular scheme employed.

The pressure terms in Eqs. (2) and (3) are approximated as

$$DPDX = \left.\frac{\partial p}{\partial x}\right|_{i,j} = \frac{p_{i+1,j} - p_{i,j}}{(1/2)(\Delta x_i + \Delta x_{i+1})} \tag{11}$$

$$DPDY = \left.\frac{\partial p}{\partial y}\right|_{i,j} = \frac{p_{i,j+1} - p_{i,j}}{(1/2)(\Delta y_j + \Delta y_{j+1})}. \tag{12}$$

The diffusion terms are

$$DIFU = \nu\left(\frac{\partial^2 u}{\partial x^2} + \frac{\partial^2 u}{\partial y^2}\right) \tag{13}$$

$$DIFV = \nu\left(\frac{\partial^2 v}{\partial x^2} + \frac{\partial^2 v}{\partial y^2}\right) \tag{14}$$

$$DIFF = \Gamma_\phi\left(\frac{\partial^2 \phi}{\partial x^2} + \frac{\partial^2 \phi}{\partial y^2}\right). \tag{15}$$

First-order accurate central difference discretized forms of these terms for non-uniform grid can be obtained using Taylor series expansion. The finite difference forms of the basic equations are, therefore, given by

$$\frac{u_{i,j} - u^n_{i,j}}{\Delta t} = -DPDX^n - DUUDX^n - DVUDY^n + DIFU^n \tag{16}$$

$$\frac{v_{i,j} - v^n_{i,j}}{\Delta t} = -DPDY^n - DUVDX^n - DVVDY^n + DIFV^n \tag{17}$$

$$\frac{\phi_{i,j} - \phi^n_{i,j}}{\Delta t} = -DUFDX^n - DVFDY^n + DIFF^n. \tag{18}$$

Superscripts n and (blank) are used to denote values at time-level t and $t + \Delta t$, respectively. The solution algorithm consists of a time-march procedure. At each step of the march, scalars are calculated explicitly from the scalar transport

equation whereas the velocity guesses are calculated explicitly from their respective conservation of momentum equations. The newly calculated velocities are considered to be first approximations at the new time level, since the continuity requirement has not yet been imposed. The approximations are improved in an iterative fashion, adjusting the cell pressures and velocities to satisfy the continuity equation. When convergence is achieved, current values of pressure and velocities are accepted and taken as initial values for the next time step. Boundary conditions are imposed on the scalar after each time step and on the velocities after each time step and after each pass through the mesh during pressure iterations. Convergence to the steady-state solution is established by taking many forward time steps. The choice of time increment must be restricted (for stability) in two ways. First, the fluid should not pass through more than one cell in one time step. Therefore, Δt must be less than (usually 0.25–0.33 times) the minimum cell transit time taken over all cells. Second, when a nonzero value of diffusivity is used the momentum or the scalar quantity should not diffuse more than one cell in one time step. More details about the solution algorithm and its application are available in [5, 10].

3. Differencing Schemes for the Advection Terms

3.1. *Weighted Upwind Differencing (WUD)*

The advected values at the cell faces are approximated by weighted interpolation between the two nodal values on either side of the cell faces with more weight given to the nodal value upstream of the cell face.

Considering the v-cell, for the right face,

$$VRW = [v_{i,j}\,\Delta x_{i+1}/2 + v_{i+1,j}\,\Delta x_i/2 + (\text{sgn})(\alpha)(v_{i,j} - v_{i+1,j})\,\Delta x_{i+ia}/2]/(\Delta x_i + \Delta x_{i+1})/2, \tag{19}$$

where $\text{sgn} = UR/|UR|$ and $ia = (1 - \text{sgn})/2$ and $0 < \alpha < 1$ is the donor cell weighting factor. If $\alpha = 0$ then central difference is obtained and if $\alpha = 1$ then full upwind difference is obtained. In general, α should be slightly greater than $\max\{|u|\,\Delta t/\Delta x, |v|\,\Delta t/\Delta y\}$. In this study α is taken as 0.6. For the top face,

$$VTW = \tfrac{1}{2}[v_{i,j} + v_{i+1,j} + (\text{sgn})(\alpha)(v_{i,j} - v_{i+1,j})], \tag{20}$$

where $\text{sgn} = VT/|VT|$.

Similar expressions can be obtained for (VLW, VBW), (URW, ULW, UTW, UBW), and (ϕRW, ϕLW, ϕTW, ϕBW) by considering the respective cells.

3.2. *Predictor–Corrector Second-Order Upwind Differencing (SOUD1)*

This scheme is essentially another version of WUD. For computations of the velocity components, a double pass through the momentum equation is taken at every time step before the pressure iteration. In the first pass the donor cell coefficient α is taken as 1.0. The computed velocities are then considered as the predicted velocities (with first order accuracy). In the second pass the predicted velocities

are used in the computation as the previous time-level velocities with $\alpha = -1.0$. Then the resulting velocities from the two calculations are averaged to obtain the new time-level velocities for pressure iteration. Computation for a scalar is done similarly by double pass through the transport equation.

These approximations are considered to be second-order accurate [6] in time and space because the first pass uses values at time level n, while the second pass uses (first-order) approximations for values at time $n+1$. The average then has the level $n+\frac{1}{2}$, which is second-order accurate in Δt. Likewise, using $\alpha = 1.0$ in the first pass and $\alpha = -1.0$ in the second pass, results in an average value of zero which is second order in space.

3.3 *Second-Order Upwind Differencing (SOUD2)*

The advected values of u, v, and ϕ at the cell faces are approximated by linear extrapolation to the cell face of two successive immediate upstream nodal values. For illustration the v-cell is considered:

$$VRW = (1+r)\, v_{i+ia,j} - r v_{i-1+3ia,j}, \tag{21}$$

where $ia = (1 - UR/|UR|)/2$ and $r = [(\Delta x_{i+ia})/2]/[(\Delta x_{i-1+2ia} + \Delta x_{i+2ia})/2]$;

$$VBW = (1+r)\, v_{i,j-1+ja} - r v_{i,j-2+3ja}, \tag{22}$$

where $ja = (1 - VB/|VB|)/2$ and $r = [(\Delta y_j)/2]/[\Delta y_{j-1+2ja}]$.

Similar expressions can be obtained for other advected quantities by considering the respective cell. This approximation, however, is not an exact transformation of the point discretization form used by Shyy [4], which is not appropriate for a staggered grid system.

3.4. *Skew Upwind Differencing (SUD)*

The advected values of u, v, and ϕ at the cell faces are approximated by considering the direction of the velocity vector at the cell face and interpolating between the values at two appropriate nodes among the nodes surrounding the cell face. The two appropriate nodes are selected by going upstream along the direction of the velocity at the cell face all the way back to the line joining the centers of the adjacent cells as shown in Fig. 2. Considering the left face of the p-cell, the approximation for ϕLW is made as follows:

$$is = UL/|UL|, \qquad ia = (1-is)/2, \qquad js = VL/|VL|, \qquad ja = (1-js)/2$$

$$\xi = \Delta x_{i-1+ia}/2, \qquad \eta = (\Delta y_j + \Delta y_{j-js})/2,$$

$$\theta = \arctan(|VL/UL|), \qquad \alpha = \arctan(\eta/\xi), \qquad \delta = \xi \tan\theta, \qquad \zeta = (is)\,\eta \cot\theta$$

$$\phi LW = \begin{cases} [(\eta-\delta)\,\phi_{i-1+ia,j} + \delta\phi_{i-1+ia,j-js}]/\eta, & \text{if } \alpha \geqslant \theta \\ \dfrac{[(\Delta x_i/2+\zeta)\,\phi_{i-1,j-js} + (\Delta x_{i-1}/2-\zeta)\,\phi_{i,j-js}]}{(\Delta x_{i-1}+\Delta x_i)/2}, & \text{if } \alpha < \theta. \end{cases} \tag{23}$$

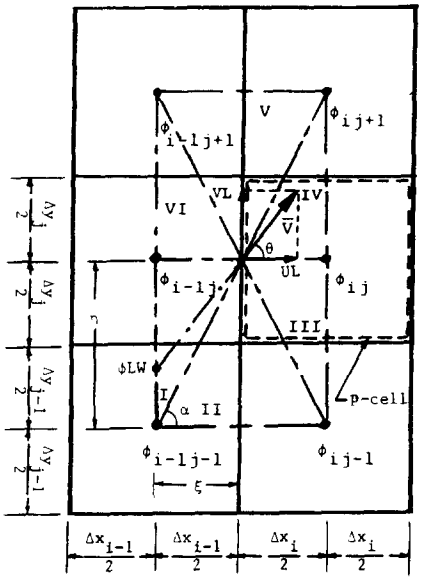

FIG. 2. Illustration of the skew upwind differencing.

Depending on the direction of the velocity vector at the cell face, there are six possible pairs of nodes between which ϕLW may have to be interpolated. Similar expressions for other advected quantities may be derived.

3.5. *Transportive Upwind Differencing (TUD)*

In this scheme the advected values are approximated by interpolating between the values of the two nodal points on either side of the cell faces [7]. The point of interpolation is selected according to the magnitude and direction of the respective component of the face velocity at a distance ξ. As illustrated in Fig. 3, this distance is evaluated as a function of the cell face velocity and time; $\xi = \beta(\Delta t/2)$ (component of face velocity). The factor β is an adjustable parameter. Hirt's stability analysis of the scheme applied to a linearized model advection equation shows that it should be equal to 1.0 to avoid numerical diffusion. This value, however, introduces oscillations to the solution which can be eliminated to some extent by taking it slightly larger than 1.0 at the expense of introducing artificial diffusion. In this study it is taken as 1.0.

Considering the u-cell,

$$ULW = u_{i,j} + \frac{u_{i,j} - u_{i-1,j}}{\Delta x_i}\left[-\frac{\Delta x_i}{2} - \beta(UL)\frac{\Delta t}{2}\right] \tag{24}$$

$$UTW = u_{i,j} + \frac{u_{i,j+1} - u_{i,j}}{(1/2)(\Delta y_j + \Delta y_{j+1})}\left[\frac{\Delta y_j}{2} - \beta(VT)\frac{\Delta t}{2}\right]. \tag{25}$$

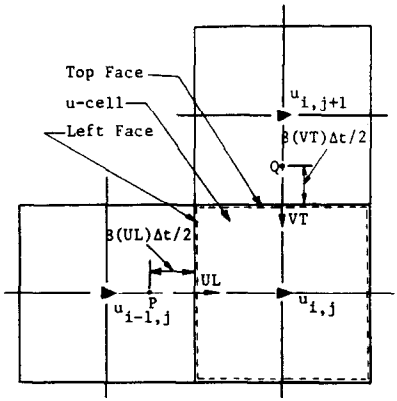

FIG. 3. Illustration of the transportive upwind differencing.

Similar expressions for other advected quantities can be obtained considering the respective cell.

3.6. *Directional Transportive Upwind Differencing (DTUD)*

This scheme is a combination of transportive and skew upwind differencing. The magnitude and direction of the velocity vector at the cell face under consideration are taken into account; and the advected values are approximated by interpolating among the properties at four nodal points surrounding the point of interpolation. The four nodal points are selected by considering the direction of the velocity vector at the cell face and the point of interpolation is chosen at a distance $\beta(\Delta t/2)\,|\bar{V}|$ upstream in the direction of the velocity vector $\bar{V}$, as illustrated in Fig. 4. Considering the left face of the cell (i,j) and assuming the direction of the velocity vector $\bar{V}_L$, the advected value is interpolated at the point P from the values at nodes $(i-1,j-1)$, $(i,j-1)$, $(i-1,j)$, and (i,j). Considering the top face, the advected value is interpolated at the point Q from the values at nodes $(i-1,j)$, (i,j), $(i-1,j+1)$, and $(i,j+1)$, if the direction of the velocity is as indicated.

Figure 4 shows that the point P is located at $(\xi=\beta(UL)\,\Delta t/2,\ \eta=\beta(VL)\,\Delta t/2)$. There are four possible locations of P depending on the direction of UL and VL. The coefficient β is an adjustable parameter identical to that of TUD parameter and has a value of 1.0 which eliminates numerical diffusion but introduces oscillations to the solution. The approximation for ϕLW can be made as follows;

$$js = VL/|VL|, \qquad ja = (1-js)/2$$

$$\xi = [\Delta x_i/2 + \beta(UL)\,\Delta t]/(\Delta x_{i-1} + \Delta x_i)/2, \qquad \eta = \beta\,|VL|\,\Delta t/(\Delta y_j + \Delta y_{j-js})/2$$

$$\phi LW = (1-\xi)(1-\eta)\,\phi_{i,j} + \xi(1-\eta)\,\phi_{i-1,j} + (1-\xi)\,\eta\phi_{i,j-js} + \xi\eta\phi_{i-1,j-js}. \quad (26)$$

Similar expressions for other advected values can also be obtained.

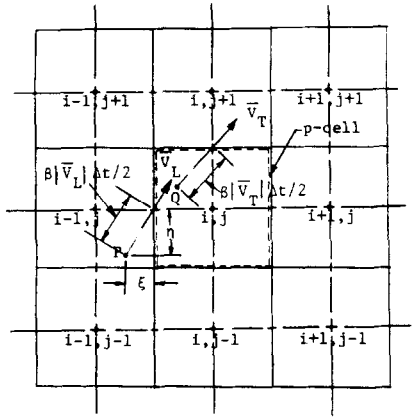

FIG. 4. Illustration of the directional transportive upwind differencing.

3.7. *Quadratic Upwind Interpolation Differencing (QUID)*

The advected values at the cell faces are approximated by quadratic interpolation among the respective values at three nodes; two located on both sides of the face and the third one is chosen at one cell width away from either of these two nodes depending on the direction of respective component of the face velocity.

Considering the u-cell,

$$URW = a\delta^2 + b\delta + c, \tag{27}$$

where

$$a = \frac{(ru_{i+1+ia,j} + u_{i-1+ia,j})/(r+1) - u_{i+ia,j}}{\Delta x_{i+ia}\,\Delta x_{i+1+ia}}$$

$$b = \frac{(r^2 u_{i+1+ia,j} - u_{i-1+ia,j})/(r+1) - (r-1)\,u_{i+ia,j}}{\Delta x_{i+ia}}$$

$$c = u_{i+ia}$$

$$\delta = (\text{sgn})\,\Delta x_{i+1}/2, \qquad r = \Delta x_{i+ia}/\Delta x_{i+1+ia}$$

$$\text{sgn} = UR/|UR|, \qquad ia = (1 - \text{sgn})/2.$$

Similarly,

$$UBW = a\delta^2 + b\delta + c, \tag{28}$$

where

$$a = \frac{(ru_{i,j+ja} + u_{i,j-2+ja})/(r+1) - u_{i,j-1+ja}}{\Delta v_{j-2+ja}\,\Delta v_{j-1+ja}}$$

$$b = \frac{(r^2 u_{i,j+ja} - u_{i,j-2+ja})/(r+1) - (r-1)\,u_{i,j-1+ja}}{\Delta v_{j-2+ja}}$$

$$c = u_{i,j-1+ja}$$

$$\delta = (\text{sgn})\,\Delta y_{j-1+ja}/2, \qquad r = \Delta v_{j-2+ja}/\Delta v_{j-1+ja}, \qquad \Delta v_j = (\Delta y_j + \Delta y_{j+1})/2$$

$$\text{sgn} = VB/|VB|, \qquad ja = (1 - \text{sgn})/2.$$

Similar expressions for other advected values can also be obtained.

4. Test Cases

The three test cases chosen for the evaluation of the selected discretization schemes are:

1. The transport of a scalar step in a uniform velocity field at angles of 26.6 and 45° to the grid lines.

2. Two interacting parallel streams with different velocities at angles of 26.6 and 45° to the grid lines.

3. A two-dimensional slot-jet with the jet axis skewed at angles 0, 26.6, and 45° to the grid lines.

The flow in all cases is laminar to avoid the question of the reliability of turbulence models and whether the diffusion is introduced by the differencing scheme or the eddy viscosity. The flow direction considered mostly in the study is skewed at an angle to the grid lines since numerical diffusion is known to be predominant then. Analytical solutions are available for cases 1 and 2 to assess the accuracy of the scheme. All of the schemes are subjected to the same boundary and initial conditions, stability criteria, and solution procedure. Hence, stability problems that some schemes may develop will be inherent in the differencing schemes used for the advection terms. Initial values of the velocity components are taken as zero. Computations are carried out for pure advection ($|Pe| = \infty$) and advection dominated flows (Peclet numbers of about 200 and 20) for all the test cases. The difference in the results for $|Pe| = \infty$ and for $|Pe| \sim 200$, however, is not significant. Therefore, the results for cases with $|Pe| \sim 200$ are not presented here. Uniform square grids of

size 0.01 m × 0.01 m are used for all the test cases. In the following sections, s and n represent the directions along and normal to the flow direction, respectively.

4.1. *Transport of a Scalar Step*

This test case examines the transport of a line source for a scalar step downstream in a uniform velocity field. Since the advective velocities are constant, the transport equation is linear for this case. Thus, the effect of skewness of the velocity field to the grid lines can be studied without considering the nonlinearity of the transport equation.

The input profile at the inlet is a scalar step profile specified as

$$\phi(0, n, t) = \begin{cases} 0.0, & -h/2 < n < 0 \\ 1.0, & 0 < n < h/2, \end{cases}$$

where h is the width of the flow domain. For the pure advection case ($\Gamma_\phi = 0.0$), the steady-state profiles downstream should be the same as the input profile if numerical diffusion is absent. For the case of nonzero diffusivity, the steady-state analytical solution is given by [3]

$$\phi(s, n) = 0.5\left[1 + \operatorname{erf}\left\{-n\left(\frac{V}{4\Gamma_\phi s}\right)^{1/2}\right\}\right], \tag{29}$$

where V is the magnitude of the resultant uniform velocity in the flow direction.

For the flow angle 26.6° to the grid lines, a 40 × 45 mesh is used with $\Delta t = 0.001$ s. The schematic of the test case is shown in Fig. 5. Analytical as well as predicted steady-state profiles are presented in Figs. 6 and 7 for Peclet numbers of ∞ and 22.36. The profiles are at a distance $s/\Delta = 13$ from the inlet section, where Δ is the grid size. The figures show that for the Peclet numbers considered, WUD suffers the

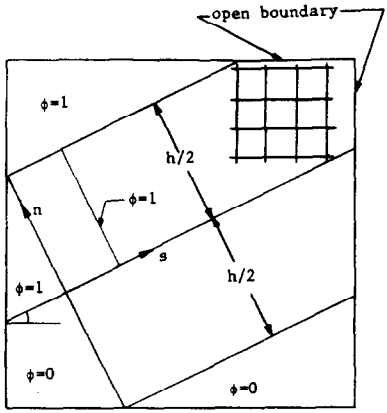

FIG. 5. Schematic of the first test case—advection of a scalar step in a uniform velocity field at an angle to the grid line.

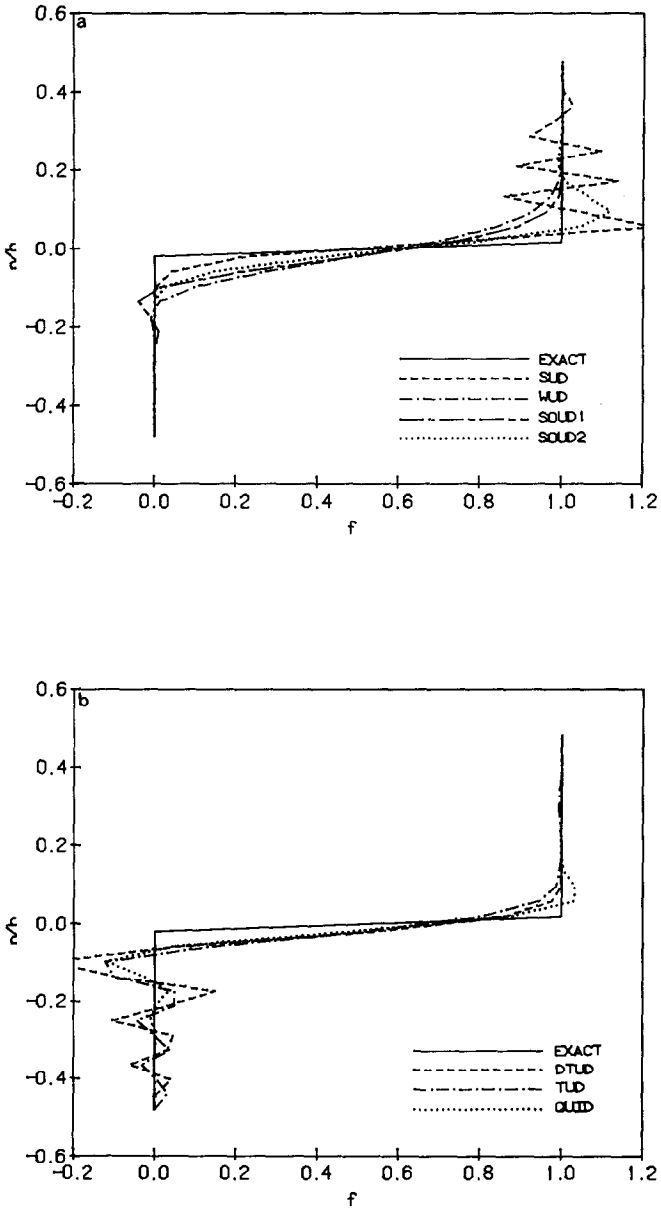

FIG. 6. Transport of a scalar step; predicted scalar step profiles for the first test case ($s/\Delta = 13$, $|Pe| = \infty$, flow angle = 26.6°).

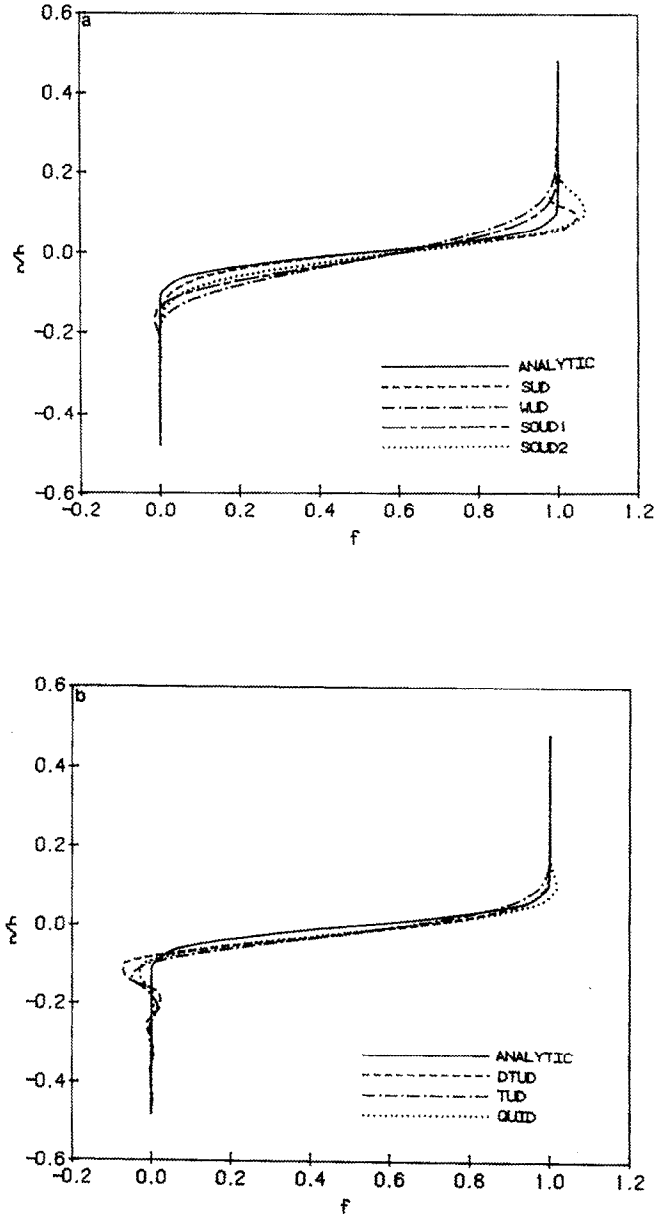

FIG. 7. Transport of a scalar step; predicted scalar step profiles for the first test case ($s/\Delta = 1$ $|Pe| = 22.36$, flow angle $= 26.6°$).

most numerical diffusion which in turn supresses any oscillation in the solution. Other schemes suffer more or less from oscillations which are significant for pure advection case ($|Pe| = \infty$). At $|Pe| = 22.36$, oscillations are less severe. At all Peclet numbers, SUD, SOUD2, TUD, DTUD, and QUID schemes have less numerical diffusion than WUD and SOUD1 and the accuracy of the solutions is similar.

For the flow angle of 45°, a 40×40 mesh is used with $\Delta t = 0.001$ s. Predicted steady-state profiles at $s/\Delta = 13$ for $|Pe| = \infty$ and 21.21 are shown in Figs. 8 and 9. In this case SUD has very little numerical diffusion and does not produce any overshoot or oscillation. Other schemes, namely DTUD, TUD, QUID, and SOUD2, have similar numerical diffusion and accuracy and produce overshoots which are less severe than those at 26.6°. WUD and SOUD1 suffer from more numerical diffusion and produce no oscillations.

The normalized total errors produced by SUD, SOUD2, DTUD, and QUID for this test case with zero diffusivity are presented in Table I. The errors are estimated using the normalized deviation defined by

$$N.D. = \frac{\int_{-h/2}^{h/2} |\phi_e - \phi_c| \, dh}{\int_{-h/2}^{h/2} |\phi_e| \, dh},$$

where ϕ_e and ϕ_c are the exact and computed solutions, respectively. The table shows that, at 26.6° flow angle, the error is maximum for SUD. This is largely due to the numerical dispersion or oscillations. Syed and Gosman [1] showed that for SUD, numerical diffusion error approaches zero around a flow angle of 26°. The oscillations can be eliminated if the scheme is bounded as will be shown in Section 5. At a 45° flow angle, SUD produced the minimum error among the four schemes, which is expected. Leschziner [3] showed that, for SUD, at this flow angle with uniform square grid, numerical diffusion occurs only in the streamwise direction. Since the flow is advection dominated, diffusive transport in the streamwise direction is unimportant and numerical diffusion is of little consequence [3].

TABLE I

Normalized Deviation Errors in Percent for the First Test Case with $|Pe| = \infty$

	Flow angle	
Scheme	26.6°	45°
SOUD2	3.3	10.9
DTUD	6.4	6.8
QUID	2.5	8.0

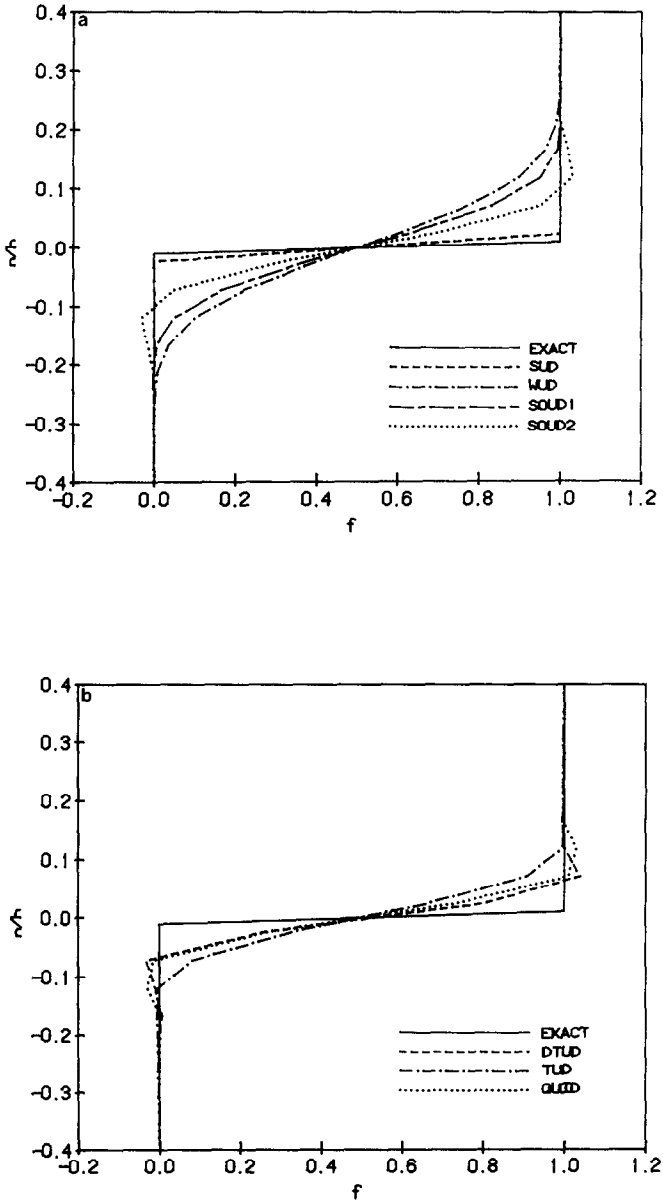

FIG. 8. Transport of a scalar step; predicted scalar step profiles for the first test case ($s/\Delta = 13$, $|Pe| = \infty$, flow angle = 45°).

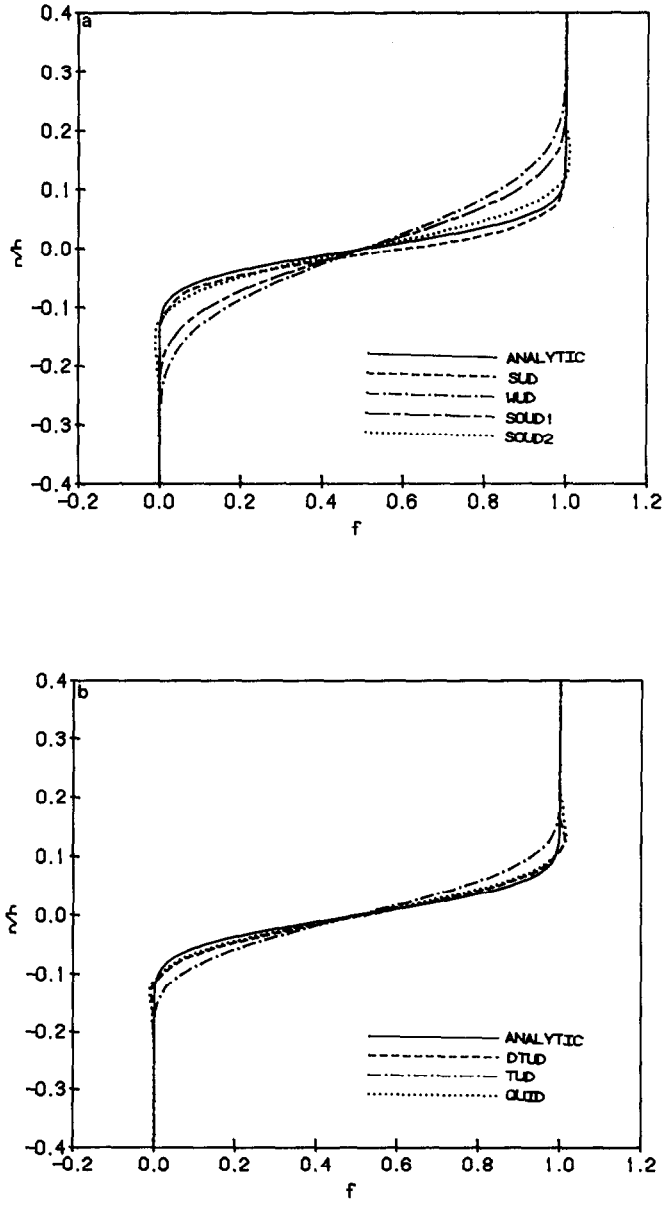

FIG. 9. Transport of a scalar step; predicted scalar step profiles for the first test case ($s/\Delta = 13$, $|Pe| = 22.36$, flow angle $= 45°$).

4.2. *Interaction of Two Parallel Streams*

The interaction of two parallel streams of different velocities moving at an angle of 26.6 and 45° to the grid lines is considered. Since the advecting velocities for this test case are also functions of space and time, the momentum transport equations are nonlinear.

A schematic for this test case is shown in Fig. 10. The velocity ratio between the two parallel streams is 2.0. For pure advection ($\nu = 0.0$) the steady-state velocity profiles at downstream locations should be the same if numerical diffusion is absent. For nonzero viscosity, the analytical solution of the velocity distribution (similarity profile) by Schlichting [11] is used for comparison.

A 38×43 mesh is used for the flow angle of 26.6° with $\Delta t = 0.001$ s. The Peclet numbers considered are ∞ and 22.36 based on the higher velocity of the two streams. The predicted profiles at a distance $s/\Delta = 13$ from the inlet section are presented in Figs. 11 and 12. The figures show that SUD, TUD, and DTUD exhibit significant oscillations in the profile for pure advection ($|Pe| = \infty$). The results of TUD, DTUD, and QUID show comparable accuracy. WUD exhibits the most numerical diffusion with no oscillation. SOUD1 and SOUD2, on the other hand, introduce moderate numerical diffusion and moderate oscillations.

A 38×38 mesh is used for the 45° flow angle with $\Delta t = 0.001$ s. Computation is carried out for two Peclet numbers (∞ and 18.86) based on the higher velocity of the streams. The predicted and exact or analytical profiles are presented in Figs. 13 and 14. At this flow angle none of the schemes, except QUID, produces significant oscillations. The velocity profile predicted using QUID at $|Pe| = \infty$ (Fig. 13) is shown at 150 time steps. With further advances in time the solution diverges.

4.3. *Two-Dimensional Slot Jet*

The third test case considered is a two-dimensional laminar jet issuing from a wall into a stagnant surrounding. Predicted profiles for the axial velocity of the jet

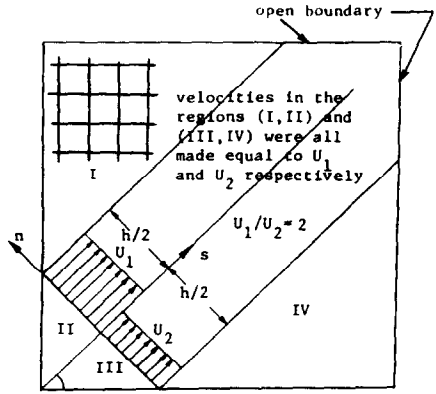

FIG. 10. Schematic of the second test case—interaction of two parallel streams skewed at an angle to the grid lines.

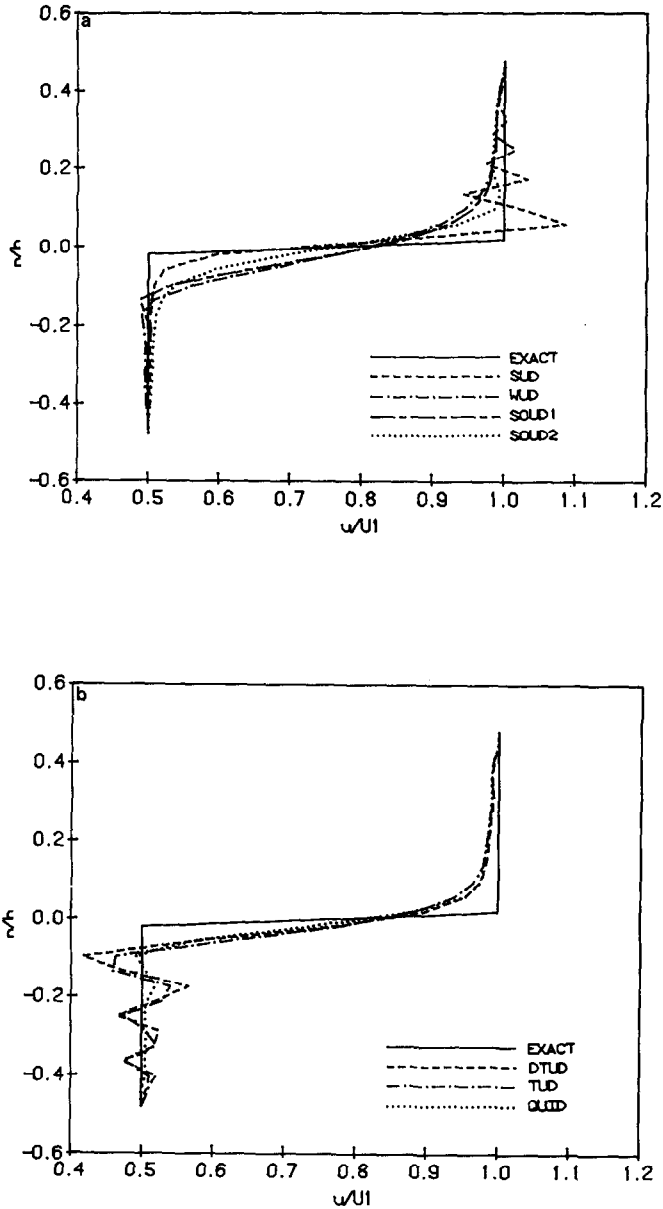

FIG. 11. Interacting parallel streams; predicted velocity profiles for the second test case ($s/\Delta = 13$, $|Pe| = \infty$, flow angle $= 26.6°$).

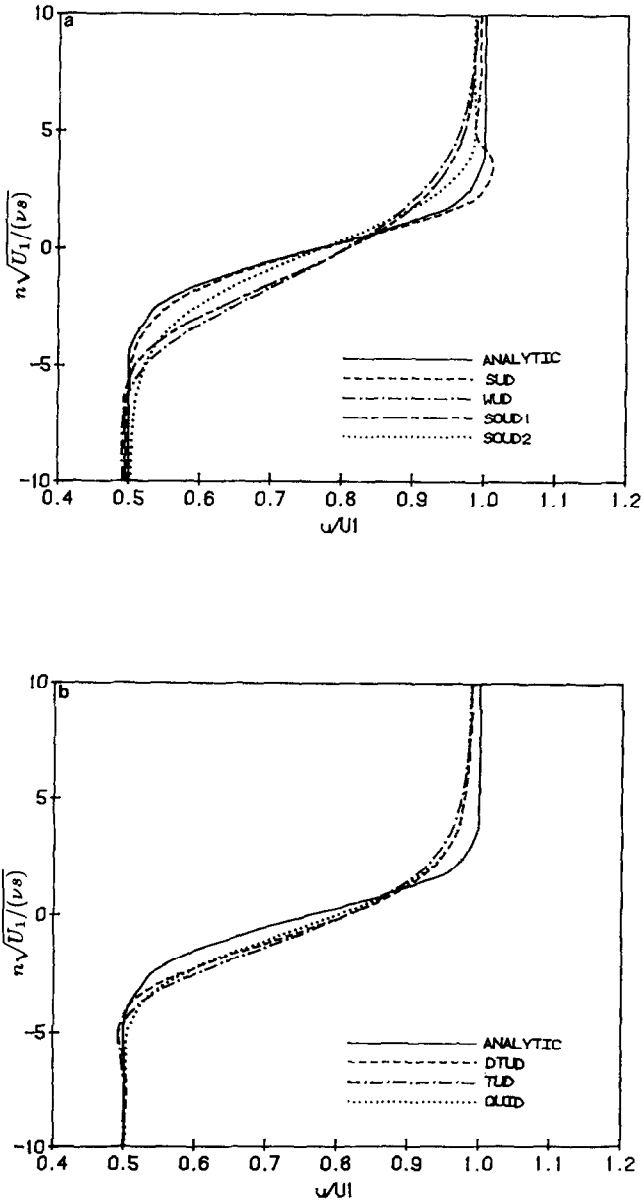

FIG. 12. Interacting parallel streams; predicted velocity profiles for the second test case ($s/\Delta = 13$, $|Pe| = 23.36$, flow angle = 26.6°).

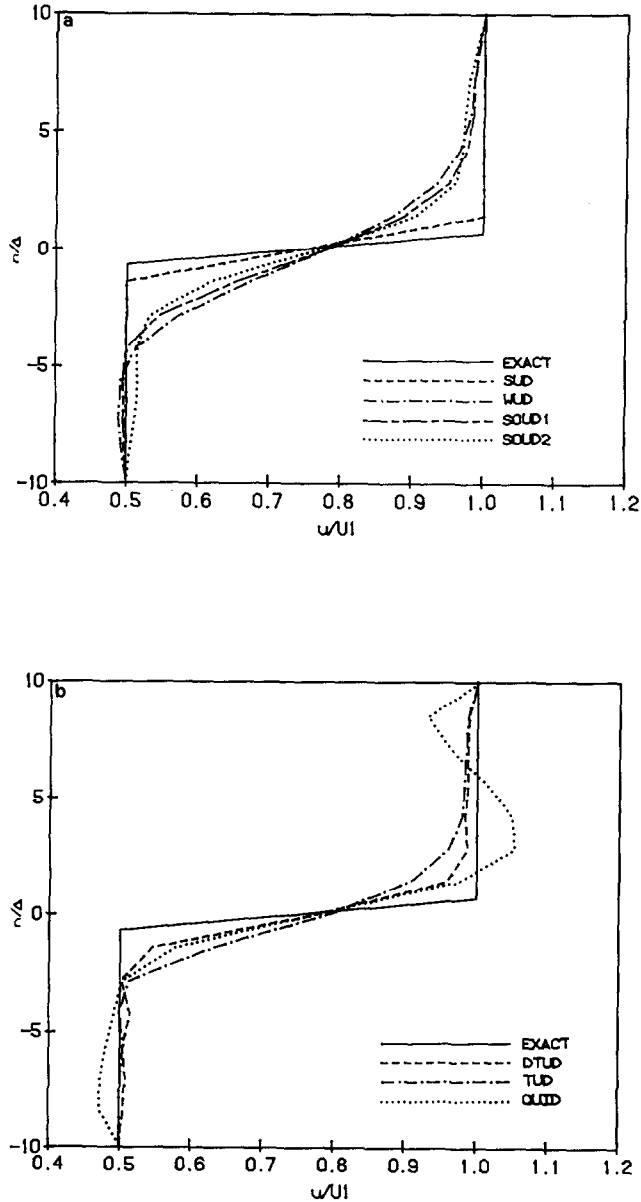

FIG. 13. Interacting parallel streams; predicted velocity profiles for the second test case ($s/\Delta = 13$, $|Pe| = \infty$, flow angle $= 45°$).

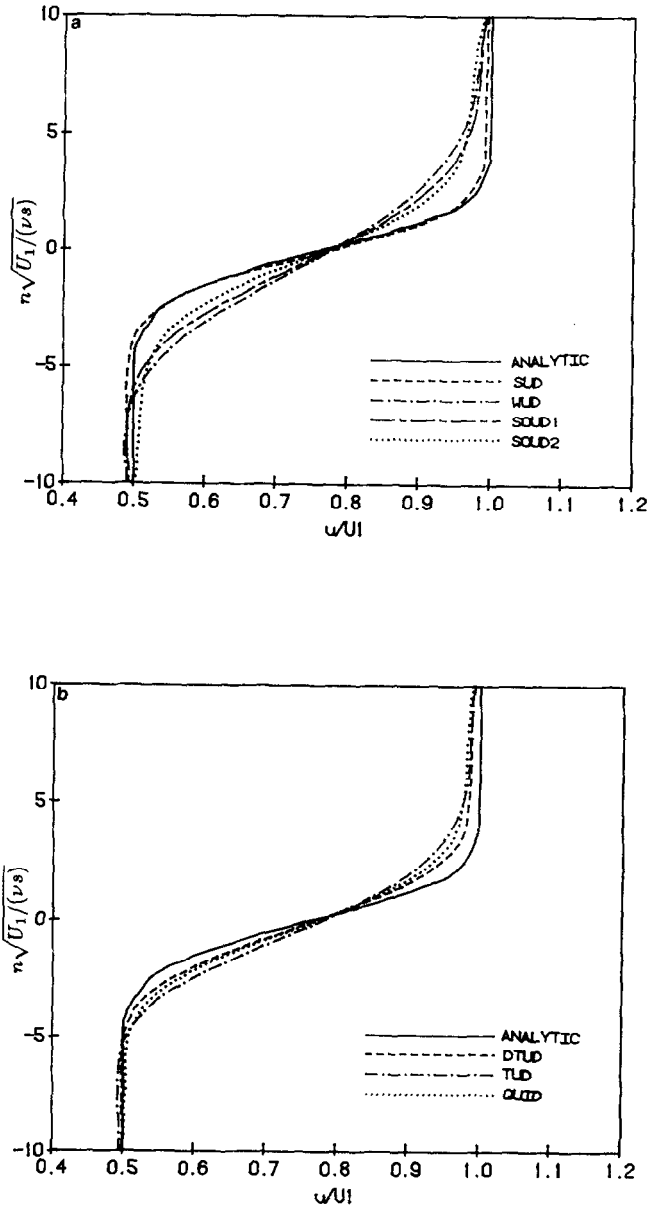

FIG. 14. Interacting parallel streams; predicted velocity profiles for the second test case ($s/\Delta = 13$, $|Pe| = 18.86$, flow angle = 45°).

at different locations along the jet axis are examined. Starting from $t = 0$ and $s = 0$ the jet advances several jet widths downstream and eventually reaches steady-state condition. The width of the jet at the entrance spreads over four cells. Three angles of inclination of the jet axis to the grid lines (0, 26.6, and 45°) are considered. Results for flows at two different Peclet numbers (∞ and 33.3, based on the jet exit velocity) are presented. Two criteria are considered for comparison of the predicted steady-state profiles; the outward spread of the jet (in the normal direction to the jet axis) and the center line velocity of the jet. For pure advection the profiles are compared with the inlet profile at the jet exit. For flow at $|Pe| = 33.3$, the steady-state profiles for nonskewed jet are virtually scheme independent and thus can be considered exact [3] for the purpose of comparison (instead of the exact solution) with the predicted profiles of a skewed jet possessing the same width and velocity at the jet exit as that of the nonskewed jet. Transient profiles are used to observe the transient solution behavior and stability of the schemes.

A 50×40 mesh is used for the nonskewed jet with $\Delta t = 0.0005$ s. Predicted steady-state velocity profiles for the pure advection case are shown in Fig. 15 at location $s/\Delta = 20$. Although the center line velocities are more or less the same for all the schemes, TUD, DTUD, and QUID produce some undershoot near the base of the profile. The outward spread is minimal for all the schemes except for WUD and SUD. The same pattern is observed at other downstream locations. The predicted axial velocity profiles of the nonskewed jet at two axial positions are presented in Figs. 16 and 17 for $|Pe| = 33.3$. All schemes produce identical profiles at $s/\Delta = 20$ and very similar profiles at $s/\Delta = 30$. QUID shows some overshoot at $s/\Delta = 30$ which results in an asymmetry in the profile as exhibited in Fig. 17. TUD and DTUD, on the other hand, show some undershoot near the jet axis after about 100 time steps as shown in Fig. 18. This undershoot is not present in the steady-state solution. QUID also exhibits some undershoot near the jet axis, which can be considered minor compared to the undershoot produced by TUD and DTUD at the same time level. Other schemes do not exhibit any undershoot or overshoot in the transient or steady-state solutions.

A schematic of the mesh system for the skewed jet is shown in Fig. 19. A grid size of 55×75 with a $\Delta t = 0.0005$ s is used for the flow angle of 26.6°. The predicted profiles are presented in Figs. 20 and 21. The profiles are nonsymmetric about the

oscillations near the base of the profile while SUD develops overshoot near the jet axis. WUD exhibits the most numerical diffusion. The profile for SOUD1 is shown at 410 time steps, after which it becomes unstable. At $|Pe| = 33.3$, SUD, DTUD, TUD and QUID have similar accuracy when compared to the nonskewed jet profile (Fig. 21). For SUD, the computed velocity near the axis is marginally better than other schemes.

A 60×60 grid system is employed in the computation with $\Delta t = 0.0005$ s for the 45° skew angle. The computed velocity profiles for the skewed jet are shown in Fig. 22 and 23 for $s/\Delta = 20$. Although none of the schemes produce any oscillation

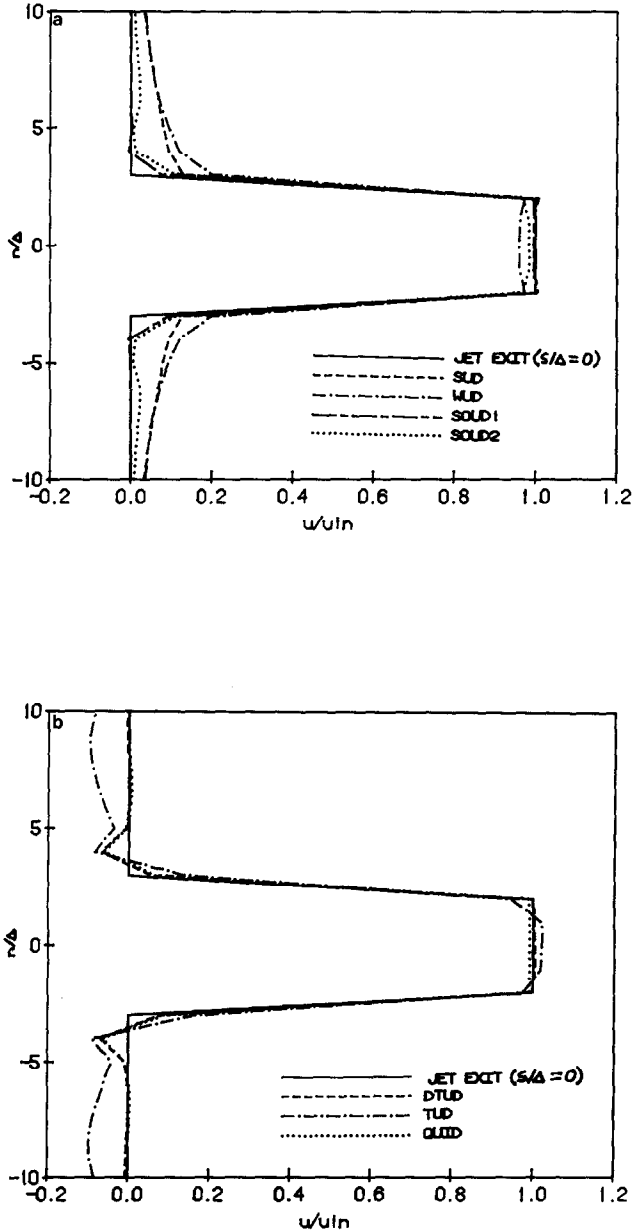

FIG. 15. Predicted velocity profiles for the third test case ($s/\Delta = 20$, $|Pe| = \infty$, 0° jet).

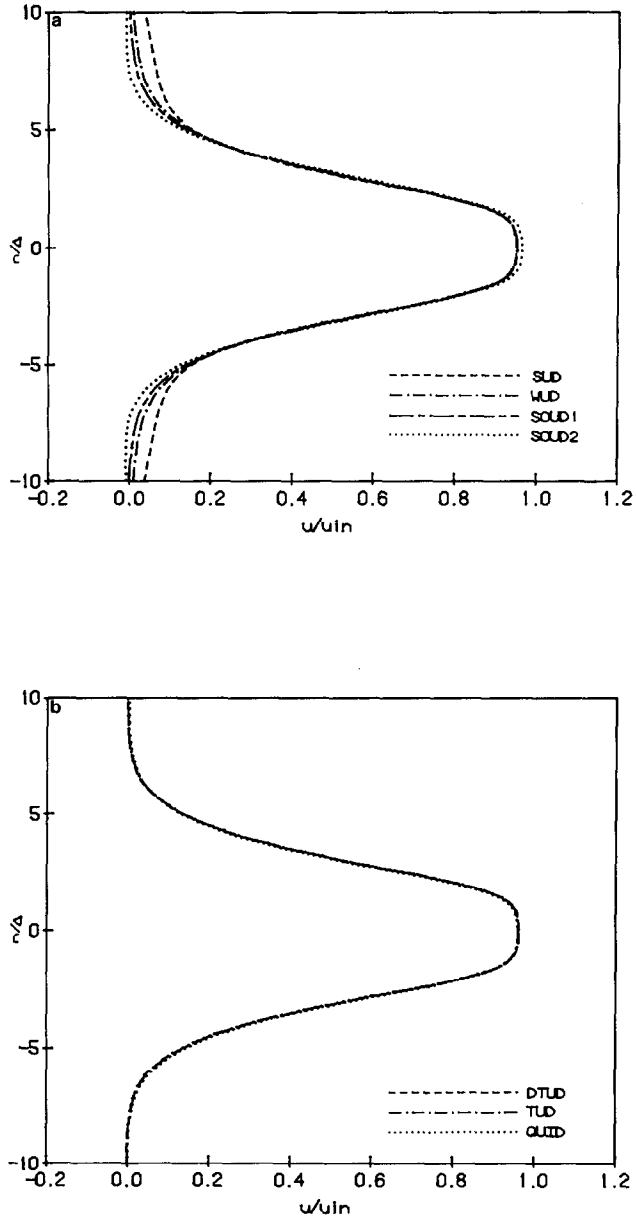

FIG. 16. Predicted velocity profiles for the third test case ($s/\Delta = 20$, $|Pe| = 33.33$, 0° jet).

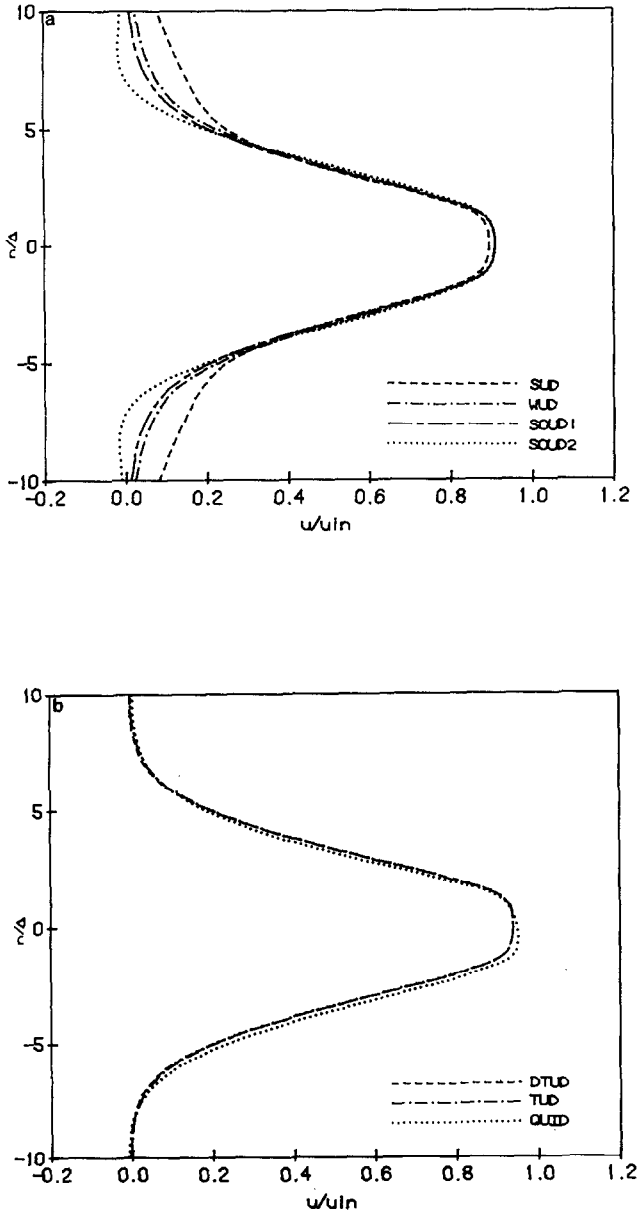

FIG. 17. Predicted velocity profiles for the third test case ($s/\Delta = 20$, $|Pe| = 33.33$, 0° jet).

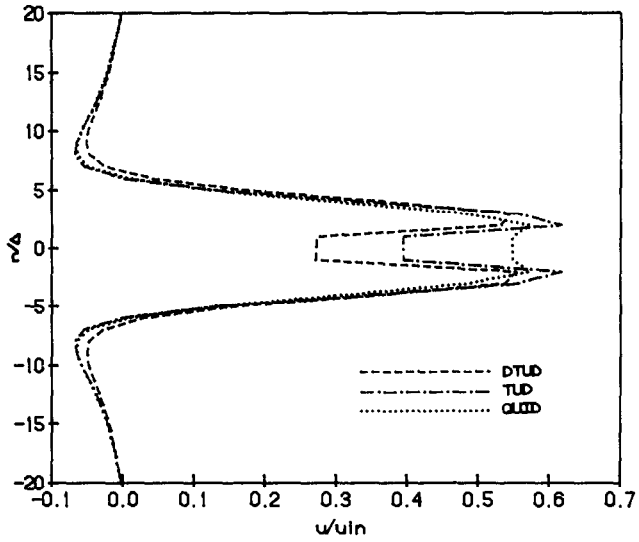

FIG. 18. Under-shoot produced by TUD, DTUD, and QUID for the non-skewed jet.

(Fig. 22) for pure advection, large numerical diffusion and outward spread is observed in the profiles when compared to the jet exit profile. SUD, however, produces less diffusion than other schemes. Figure 23 shows that all the schemes suffer, to some extent, from numerical diffusion compared to the nonskewed jet solution for $|Pe| = 33.3$. Among the seven schemes studied, WUD introduces the most numerical diffusion since the spread is more and the center line velocity is least compared to the nonskewed jet profile. For SUD, on the other hand, although the outward spread is more than some of the other schemes, the center line velocity is closer to the nonskewed jet profile than other schemes.

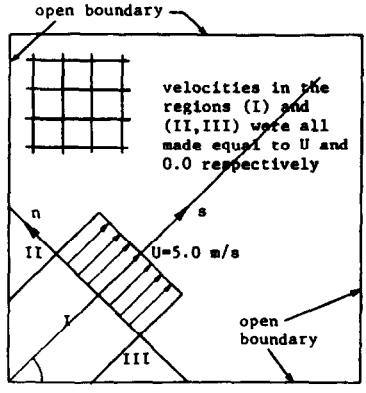

FIG. 19. Schematic of the third test case—two-dimensional jet skewed at an angle to the grid lines.

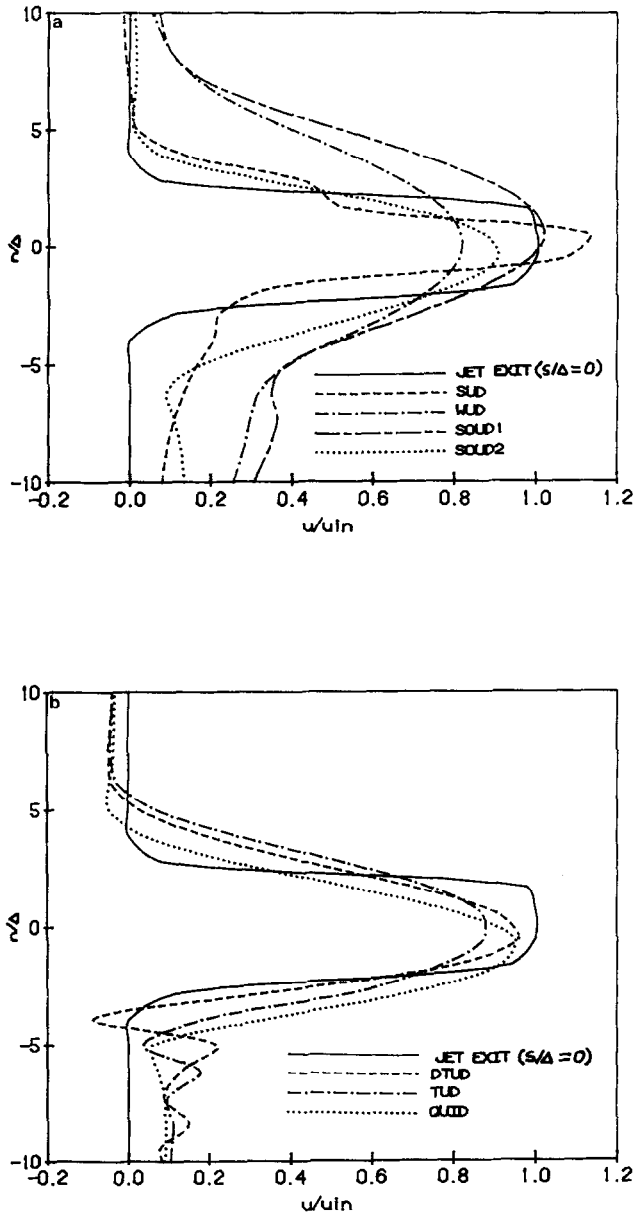

FIG. 20. Predicted velocity profiles for the third test case ($s/\Delta = 20$, $|Pe| = \infty$, 26.6° skewed jet).

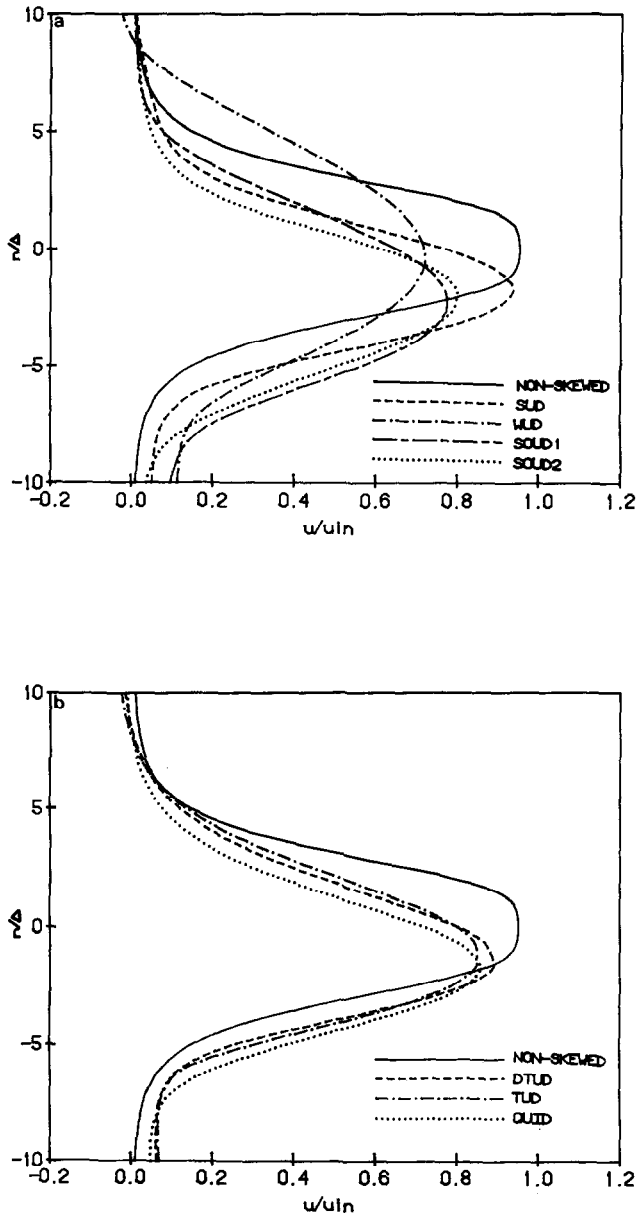

FIG. 21. Predicted velocity profiles for the third test case ($s/\Delta = 20$, $|Pe| = 33.33$, 26.6° skewed jet).

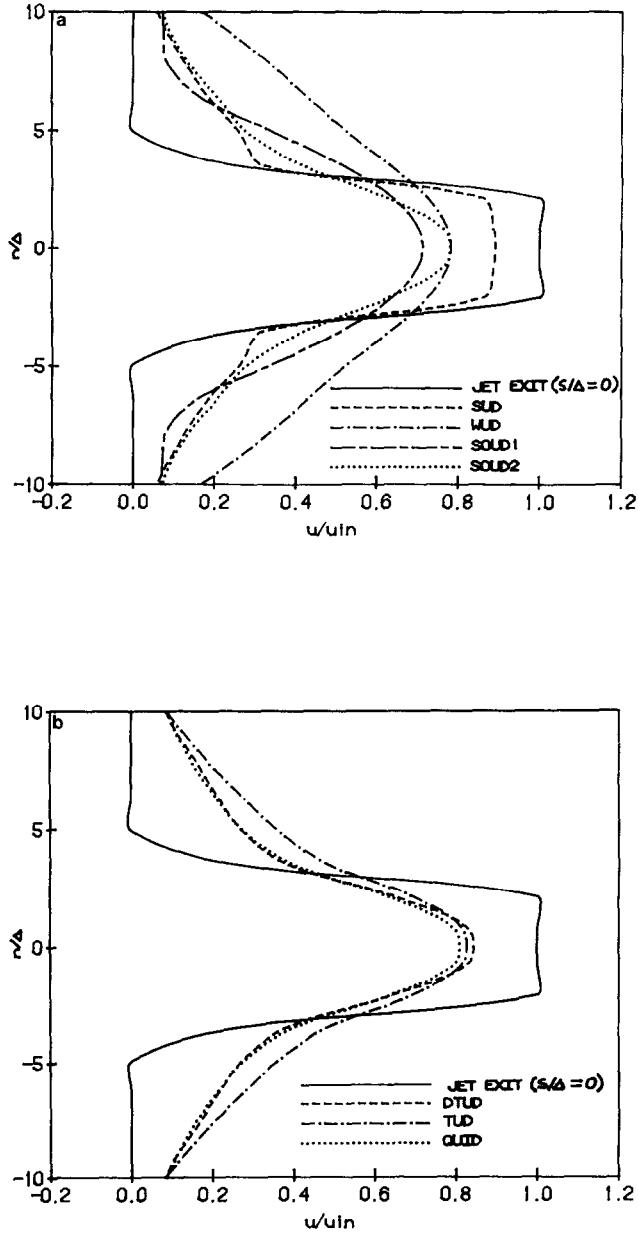

FIG. 22. Predicted velocity profiles for the third test case ($s/\Delta = 20$, $|Pe| = \infty$, 45° skewed jet).

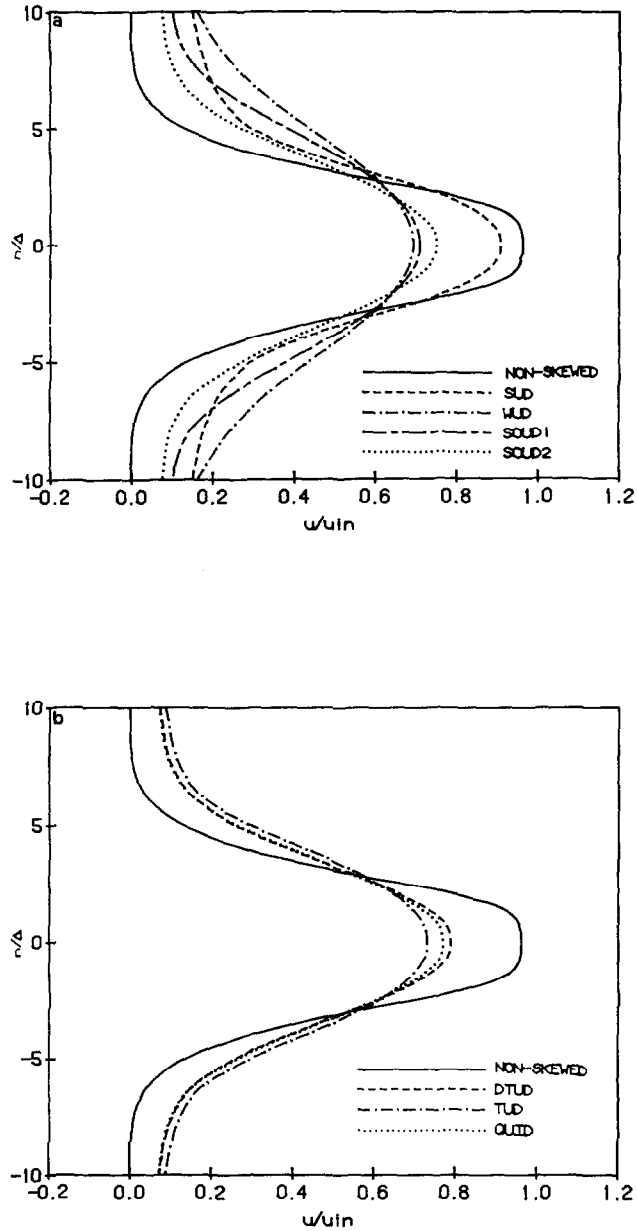

FIG. 23. Predicted velocity profiles for the third test case ($s/\Delta = 20$, $|Pe| = 33.33$, 45° skewed jet).

5. BOUNDING

It is rather obvious from this study and others [1–4] that lower order schemes such as upwind, weighted upwind, and hybird/upwind suffer from excessive numerical diffusion. Skew upwind or other higher order schemes, although more accurate, suffer from nonphysical spatial oscillations (often called overshoot). This problem can be treated using a filtering technique such as the flux-connected transport, originally proposed by Book and Boris [12, 13] and later improved by Zalesak [14], to partially or totally eliminate the oscillations and maintain accurate solutions.

Further evaluation of the higher order schemes by the authors using the filtering technique of Zalesak [14] is underway. In Zalesak's method, fluxes computed using a lower order and a higher order scheme are blended to compute the advection terms so that the oscillations are eliminated. Figure 24 shows the case of pure advection of a scalar step in a uniform velocity field skewed at an angle 26.6° to the grid lines. The computation is performed using SUD as the higher order scheme and full donor cell upwind differencing as the lower order scheme. The figure shows that the oscillations are significantly eliminated compared to the solution by SUD only.

Simple bounding, which is a less sophisticated but a more economical technique, produces acceptable solutions. In this case the computed value for a particular cell is compared to the computed values of its surrounding cells. Let

$$\phi_{\max} = \max(\phi_{i-1,j}, \phi_{i+1,j}, \phi_{i,j-1}, \phi_{i,j+1}) \tag{30}$$

$$\phi_{\min} = \min(\phi_{i-1,j}, \phi_{i+i,j}, \phi_{i,j-1}, \phi_{i,j+1}). \tag{31}$$

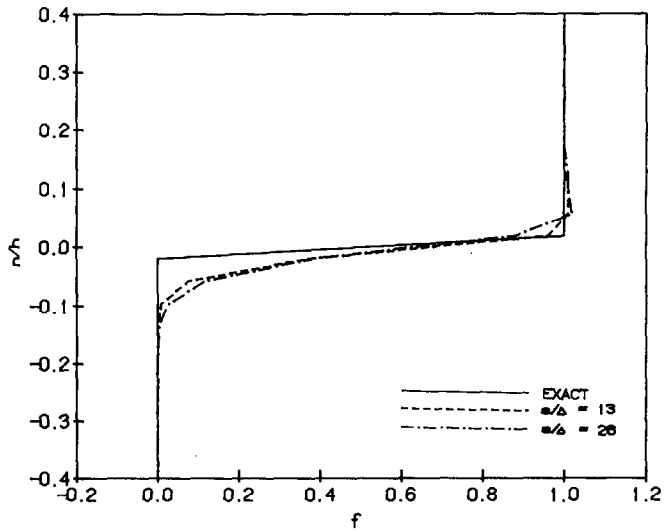

FIG. 24. Predicted scalar step profiles for the first test case using flux corrected transport technique and skew upwind differencing ($|Pe| = \infty$, flow angle = 26.6°).

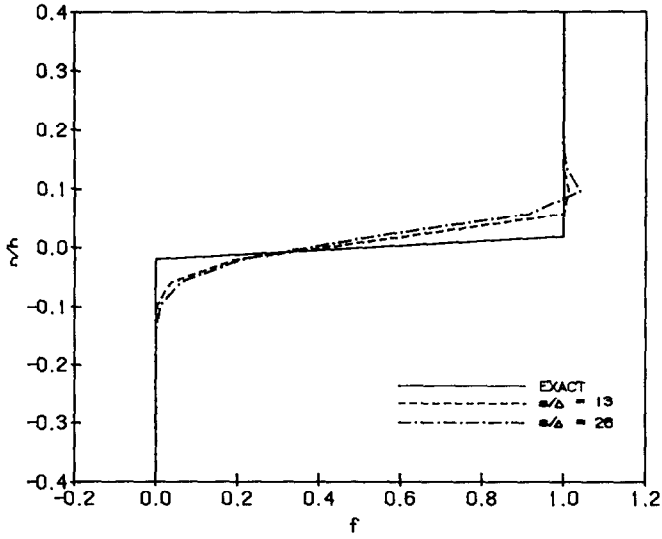

FIG. 25. Predicted scalar step profiles for the first test case using simple bounding and skew upwind differencing ($|Pe| = \infty$, flow angle = 26.6°).

If $\phi_{\min} < \phi_{i,j} < \phi_{\max}$ then $\phi_{i,j}$ is left unchanged but if $\phi_{i,j} < \phi_{\min}$ then $\phi_{i,j}$ is set equal to $\phi_{\min}$ and if $\phi_{i,j} > \phi_{\max}$ then $\phi_{i,j}$ is set equal to $\phi_{\max}$. Results, using SUD and this method, for pure advection of a scalar step in a uniform velocity field skewed at an angle of 26.6° is presented in Fig. 25, which shows that the oscillations are significantly removed.

6. CLOSURE

Seven finite-difference schemes have been evaluated to identify an accurate discretization scheme for the prediction of practical flow problems. A close look at the results presented indicates that the choice of a scheme which performs well in all situations is rather difficult. WUD introduced significant numerical diffusion in the predicted profiles. SOUD1, which uses more computer time since calcultions are repeated every time step, did not improve the solution significantly over WUD and in one instance exhibited instability (pure advection of skewed jet at 26.6°). More accurate schemes (SUD, DTUD, SOUD2, QUID, TUD) produced unacceptable over- or undershoots in the solution for pure advection and advection-dominated flows. This unboundedness is largely associated with sharp discontinuity in the advected property [15]. For nonskewed jet DTUD, TUD and QUID produced undershoots in the profile near the center line during transient solution. QUID also exhibited instability for the second test case at flow angle 45° with zero viscosity. SUD and SOUD2, however, did not exhibit any instability for the test cases con-

sidered. In general, SUD produced more accurate results in the sense that numerical diffusion was least compared to other schemes, but produced severe overshoots for a flow angle of 26.6°. SOUD2 exhibited less overshoot but produced more numerical diffusion than SUD. SOUD2 requires less computer time and implementation effort than SUD. Based on the results of the test cases, these two schemes can be considered better than other evaluated schemes. A suitable bounding or filtering technique may be used to eliminate the oscillations in the predictions. Simple bounding was found to be an economical and effective solution to the overshoot problem.

ACKNOWLEDGMENT

The authors acknowledge the reviewers' helpful comments and suggestions.

REFERENCES

1. S. SYED, A. GOSMAN, AND M. PERIC, "Assessment of Discretization Schemes to Reduce Numerical Diffusion in the Calculation of Complex Flows," Paper No. AIAA-85-0441, AIAA 23rd Aerospace Sciences Meeting, Reno, Nevada, Jan. 14–17, 1985.
2. S. SYED AND L. CHIAPPETTA, "Finite Difference Methods for Reducing Numerical Diffusion in TEACH-Type Calculations," Paper No. AIAA-85-0057, AIAA 23rd Aerospace Sciences Meeting, Reno, Nevada, Jan. 14–17, 1985.
3. M. A. LESCHZINER, *Comput. Methods Appl. Mech. Eng.* **23**, 293 (1980).
4. W. SHYY, *J. Comput. Phys.* **57**, 415 (1985).
5. C. W. HIRT, B. D. NICHOLS, AND N. C. ROMERO, Los Alamos Scientific Laboratory Report No. LA-5852, 1975 (unpublished).
6. C. W. HIRT, in *Proceedings, Numerical Methods for Partial Differential Equations Seminar, Univ. of Wisconsin*, 1978 (Academic Press, New York/London, 1978).
7. A. ERASLAN, W. LIN, AND R. D. SHARP, Oak Ridge National Laboratory Report No. ORNL/NUREG-8401, 1983 (unpublished).
8. G. D. RAITHBY, *Comput. Methods Appl. Mech. Eng.* **9**, 153 (1976).
9. B. P. LEONARD, *Comput. Methods Appl. Mech. Eng.* **19**, 59 (1979).
10. A. A. BUSNAINA AND D. G. LILLEY, "A Simple Finite Difference Procedure for the Vortex Controlled Diffuser," Paper No. AIAA-82-0109, AIAA 20th Aerospace Sciences Meeting, Orlando, Florida, Jan. 11–14, 1982.
11. H. SCHLICHTING, *Boundary-Layer Theory*, 6th ed. (McGraw–Hill, New York, 1968) p. 174.
12. J. P. BORIS AND D. L. BOOK, *J. Comput. Phys.* **11**, 38 (1973).
13. D. L. BOOK, J. P. BORIS, AND K. HAIN, *J. Comput. Phys.* **18**, 248 (1975).
14. S. T. ZALESAK, *J. Comput. Phys.* **31**, 335 (1979).
15. M. A. R. SHARIF AND A. A. BUSNAINA, in *Proceedings, ASME International Computers in Engineering Conference, Vol. 3, Chicago, Illinois, July* 1986, edited by G. Gupta *et al.* (1986), p. 217.